NEURO-GENETIC OPTIMIZATION OF MAGNETIC HYSTERESIS INTEGRATES IN ELECTROMAGNETIC SYSTEMS

AZZAOUI Seddik [a], SRAIRI Kamel [b], BENBOUZID M.E.H [c]
[a] Department of Sciences Technology, Laboratory of Microwaves Devices and Materials for Renewable Energy (DIMMER), University Ziane Achour of Djelfa, Algeria, E-mail: azzaoui_seddik@yahoo.fr
[b] Department of Electrical Engineering, Laboratory of Energy Systems Modeling (LESM), University Med khidar of Biskra, Algeria, E-mail: ksrairi@yahoo.fr
[c] Professeur des Universités Laboratoire Brestois de Mécanique et des Systèmes EA 4325 ENSIETA, Université de Brest / ENIB LBMS – IUT de Brest Rue de Kergoat, France, E-mail : m.benbouzid@ieee.org

ABSTRACT
In this work we have presented an approach for calculating the hysteresis loop of *Jiles-Atherton* model using the magnetic inductance as the independent variable is proposed to be used directly in the calculation time step finite volume applied to the numerical analysis of nonlinear magnetic fields. This model is characterized by five parameters that must be identified and optimized for better representation of the measured characteristics. The parameters set of the *Jiles–Atherton* hysteresis model identified by using a real coded genetic algorithm. The parameters identification performed by minimizing the mean squared error between experimental and simulated magnetic field curves. The method verified by applying it to an axi-symmetrical ferromagnetic system. The calculated results validated by experiences performed in a Single Sheet Tester's frame (SST). In this work, we are interested to develop a model based on feed-forward neural networks of which can describe magnetic hysteresis by taking account the influence of some external sizes.

Keywords
Magnetic hysteresis, *Jiles-Atherton* model, genetic algorithm, parameters identification, neural networks, finite volume method (FVM).

1. INTRODUCTION
Numerical electromagnetic is the theory and practice of solving electromagnetic field problems on digital computers. It reflects the general trend in science and engineering to formulate the laws of nature as computer algorithms and to simulate physical processes on digital computers. While theory and experiment remain the two traditional pillars of science and engineering, numerical modeling and simulation represent a third pillar that supports, complements, and sometimes replaces them. For this reason, the objective of this work is therefore to study for modeling, magnetic hysteresis, to integrate it into a computer code field. Modeling of magnetic hysteresis opens the way for the implementation of the hysteretic behavior of magnetic materials in the numerical analysis of nonlinear magnetic fields often encountered in the problems and engineering applications. Currently, several models are used such as the *Preisach* model, the *Stoner-Wohlfarth* model, the *Jiles-Atherton* model and some new approach built on the theory of artificial neural networks (ANN's) ... etc.. In our work we will be interested in a model that has the characteristics micro and macroscopic and it is answered in the literature. This is indeed the model of *Jiles-Atherton*. The latter model is characterized by parameters which must be identified and optimized for better representation of measured characteristics. The model attributes hysteresis *J-A* including the level of precision for many practical documents, ease of implementation in the finite volume method (MFV), and computational efficiency make it a viable choice for development work in a two-dimensional finite-volume [1], [2]. This study will choose the model best suited from the standpoint accuracy, processing speed and ease of implementation. The working hypotheses are restricted to the case of static regime and the equation that we solve axi-symmetrical in two dimensions 2-D, is the non-linear magnetodynamic. Thus, the finite element method has proved it self as an effective tool in solving differential equations, it allows another to take into account complex geometries and non-linearity's possible, only its implementation is against a fairly complicated. So we choose in our study for the finite volume method, which is less difficult to achieve and simple design. However, taking into account the problems of saturation, or nonlinearity parameter, remains difficult because of the requirement that the iterative calculation is needed then. This burden is particularly felt if duty structures or remeshing for problems involving very large matrices, or a dense network to account for skin effects, for example. The advantage of the search for alternative methods that can relieve the burden of numerical standard becomes obvious. We then present an application of multilayer neural networks for modeling the hysteresis loop, and the integration of this model in a computer code by finite volume.

2. FINITE VOLUME FORMULATION INCLUDING MAGNETIC HYSTERESIS
2.1 Basic Field Axi-Symmetrical Equations
The Writing equations (PDE's) describing electromagnetic phenomena is obtained from the fundamental equations of physics and properties of materials that make up the systems to be studied. The derivation of the finite volume equations begins with *Maxwell*'s field equations:

$$\nabla \cdot \boldsymbol{B} = 0 \quad (1)$$

$$\nabla \times \boldsymbol{H} = \boldsymbol{J} \quad (2)$$

Where $\boldsymbol{J}$ is the total current density which is the sum of the conductive current density $\boldsymbol{J_c}$ and the displacement current density $\boldsymbol{J_d}$.

The equations of *Maxwell* field are expanded to allow for the processing of magnetic hysteresis including the constitutive equation for magnetic materials. The general equation for a ferromagnetic material can be expressed as

$$\boldsymbol{B} = \mu_0 \left(\boldsymbol{H} + \boldsymbol{M} \right) \tag{3}$$

Where $\boldsymbol{M}$ is the magnetization nonlinear function, and μ_0 is the permeability in space [1]. In contrast to the use of scalar potentials, by choosing the potential A, the condition $\nabla \cdot \boldsymbol{B} = 0$ Is now identically satisfied, and the application of *Maxwell's* second equation $\nabla \times \boldsymbol{H} = \boldsymbol{J}$ leads to the following equation to solve

$$\nabla \times \left(\nu_0 \nabla \times \boldsymbol{A}(t+\Delta t) \right) = \boldsymbol{J}(t+\Delta t) + \nabla \times \boldsymbol{M}(t+\Delta t) \tag{4}$$

where $\boldsymbol{A}(t+\Delta t)$, $\boldsymbol{J}(t+\Delta t)$ and $\boldsymbol{M}(t+\Delta t)$ are, respectively, the magnetic vector potential, the current density, and the magnetization vectors at time $(t+\Delta t)$, Δt is the time step.

As it stands, this equation would not yield a unique solution, since it is always possible to add a function to $\boldsymbol{A}$ and satisfy the above equation. For now we will assume the condition $\nabla . \boldsymbol{A} = 0$ to guarantee a unique solution.

We will assume there is no variation in one direction, such that a 2 dimensional analysis will be sufficient. In particular, we will assume that the currents in the problem are normal to a plane, such that only a single component of $\boldsymbol{A}$ ($\boldsymbol{A}_\varphi$) will be necessary to obtain a solution over this plane (r-z plans). In this case, it can be seen that the gauge condition $\nabla . \boldsymbol{A} = 0$ is satisfied (since $\partial A_\varphi / \partial z = 0$ by definition).

With no variation in the azimuth direction, we can also state that $\partial V / \partial z = 0$, such that the governing equation can now be written in the 2-dimentional form (where the $\nabla \times \nabla$ equation reduces to the simpler *Laplacian* operator)

$$\begin{cases} \dfrac{\partial}{\partial z}\left(\dfrac{\nu_0}{r} \dfrac{\partial \boldsymbol{A}}{\partial z} \right) + \dfrac{\partial}{\partial r}\left(\dfrac{\nu_0}{r} \dfrac{\partial \boldsymbol{A}}{\partial r} \right) - \dfrac{\sigma}{r} \dfrac{\partial \boldsymbol{A}}{\partial t} = -\boldsymbol{J}_{ex} + \left(\dfrac{\partial \boldsymbol{M}_r}{\partial z} - \dfrac{\partial \boldsymbol{M}_z}{\partial r} \right) \\ \boldsymbol{A} = r \boldsymbol{A}_\varphi \end{cases} \tag{5}$$

2.2 *Jiles-Atherton* Model of Hysteresis

The model presented in original *J-A* [3], [4] gives the magnetization $\boldsymbol{M}$ with respect to the magnetic field external excitation $\boldsymbol{H}$. This model is based on the response of magnetic material without hysteresis losses. This is the behavior which the curve where anhysteretic $\boldsymbol{M_{an}}$ ***(H)*** can be described by a *Langevin* equation modified

$$\boldsymbol{M_{an}}(H) = M_s \left[\coth\left(\frac{\boldsymbol{H_e}}{a} \right) - \left(\frac{a}{\boldsymbol{H_e}} \right) \right] \tag{6}$$

Where *Ms* is the spontaneous magnetization (saturation) of the material corresponds to the alignment of the following times and the applied field $\boldsymbol{H}$ has *a* parameter equivalent to a magnetic field coupled to the thermal agitation energy according *Boltzmann's* statistics. *Weiss* discovered that the field acting on the time is not the external field applied, but an effective field ***He*** expressed by: $\boldsymbol{He} = \boldsymbol{H} + \alpha \boldsymbol{M}$, $\boldsymbol{H}$ is the external field of application the term $\alpha \boldsymbol{M}$ is the field interaction and α the correction factor representing the coupling between *Weiss* domains and can be determined experimentally. The constant *a* is an increasing function of temperature. To describe the hysteresis in magnetic materials, *Jiles* and *Atherton* [3], [5] have decomposed the magnetization into two components, the first is the reversible component and the second component is the irreversible

$$\boldsymbol{M} = \boldsymbol{M_{irr}} + \boldsymbol{M_{rev}} \tag{7}$$

The relationship between these two components and the anhysteretic magnetization $\boldsymbol{M_{an}}$ is obtained from physical considerations of the magnetization process is given by

$$\boldsymbol{M_{rev}} = c\,(\boldsymbol{M_{an}} - \boldsymbol{M_{irr}}) \tag{8}$$

$$\frac{d\boldsymbol{M_{irr}}}{d\boldsymbol{H_e}} = \frac{\boldsymbol{M_{an}} - \boldsymbol{M_{irr}}}{k\delta} \tag{9}$$

Model *Jiles-Atherton* can also be adapted for the determination of law behavior ***M (B)*** [2]. Thus, as for the previous model and using the fact that $\boldsymbol{B_e} = \mu_0 \boldsymbol{H_e}$, The expression of the total magnetization (7) is derived with respect to $\boldsymbol{B}$:

$$\frac{d\boldsymbol{M}}{d\boldsymbol{B}} = \frac{(1-c)\dfrac{d\boldsymbol{M_{irr}}}{d\boldsymbol{B_e}} + c\dfrac{d\boldsymbol{M_{an}}}{d\boldsymbol{B_e}}}{1 + \mu_0(1-c)(1-\alpha)\dfrac{d\boldsymbol{M_{irr}}}{d\boldsymbol{B_e}} + \mu_0 c\,(1-\alpha)\dfrac{d\boldsymbol{M_{an}}}{d\boldsymbol{B_e}}} \tag{10}$$

With: $$\frac{d\boldsymbol{M_{irr}}}{d\boldsymbol{B_e}} = \frac{\boldsymbol{M_{an}} - \boldsymbol{M_{irr}}}{\mu_0 k \delta} \tag{11}$$

In this case, five parameters *a, α, c, k* and *Ms* must be determined from experimental measurements. It is important to note that the parameters of the *Jiles-Atherton* model are theoretically the same regardless of the model used (***M (H)*** or ***M (B)***).

3. OPTIMIZATION BY ARTIFICIAL NEURAL-GENETICS

3.1 Introduction

The development of algorithms, originally dedicated to the problems of artificial intelligence (AI), such as artificial neural networks (ANN), or genetic algorithms (GA), allow their extrapolation to the problems of electromagnetic methods to relieve conventional calculation (finite element, finite volume, for example), which become very heavy when it comes to take into account phenomena such as movement or saturation. Our aim in the following paragraphs is to show how it is possible to use the learning ability of neural networks to model the hysteresis loop, taking into account the different parameters affecting the relation ***B (H)*** is invest its generalization characteristics to deal with problems of modelling without the need to restart the finite volume numerical computing, or the application of genetic techniques to deal with optimization problems, especially for the determination of electrical parameters and magnetic materials studied

3.2 Genetic Algorithms

3.2.1 Introduction

Genetic algorithms are developed for optimization purposes. They allow the search for a global extremism. These algorithms are based on mechanisms of natural selection (*Darwin*) and evolutionary genetics. A genetic algorithm evolved a population of genes using these mechanisms. It uses a cost function based on a performance criterion to calculate a "quality of adequacy" (fitness). Those most "strong" will be able to reproduce and have more offspring than others. Each chromosome consists of a set of elements called features or genes [6], [7]. The goal is to find the optimal combination of these elements gives a "fitness" maximum. At each iteration (generation of population), a new population is created from the previous population. Originally, the coding of

individuals made by transcribing the binary parameters to be optimized to form a gene. These genes are then put together to form the chromosome. However, there is an approach called actual encoding, where the functions of mutation and crossover are written to apply directly to the vector of parameters without using the binary form. These algorithms lend themselves well to give birth to hybrid methods that combine conventional methods and genetic algorithms. We selected an actual encoding, more flexible and more accurate. This avoids problems caused by the binary encoding. The actual coding also provides a direct view of the parameters throughout the evolution of the population. These operators are used genetic modification in this document as well as improvement tools presented in [8].

The implementation of the *Jiles-Atherton* model hysteresis of a magnetic material in a computer code requires the generation of the hysteresis loop each time it is necessary to calculate the magnetization from the applied magnetic field. This generation requires an exact knowledge of model parameters. We must then determine from experimental data obtained by measurement or supplied by the manufacturer of the material. The experimental test presented in this article allowed us to obtain the magnetic characteristics of soft ferromagnetic material (FeSi 3%). In this work we will use these experimental results to identify the parameters of the *Jiles-Atherton* model using stochastic optimization by genetic algorithms [9].

3.2.2 Parameters Identification Procedure

The schematic representation of the parameters identification procedure is shown in [7], [9], the first step is the characterization of the individuals that will form the population. The individuals θ are composed by the five parameters of the *J-A* model (in real coding, it is not necessary to code the variables in binary representation) [7], [10]. We consider the case where the population is given by

$$pop^n = \begin{bmatrix} M_s^{n,1} & k^{n,1} & c^{n,1} & a^{n,1} & \alpha^{n,1} \\ \vdots & \vdots & \vdots & \vdots & \vdots \\ M_s^{n,np} & k^{n,np} & c^{n,np} & a^{n,np} & \alpha^{n,np} \end{bmatrix} \quad (12)$$

Where each line represents an individual (a point in the optimization space), n is the generation, and np is the population size. The initial values assigned to the population are random values in the allowable range, as shown in Table 1. Each individual of the population is evaluated using the fitness between calculated and experimental results. That minimizes the fitness function given by [11]

$$ff(\theta) = \sum_{i=1}^{n} \left(M_s(t_i) - \hat{M}_s(t_i, \theta) \right)^2 \quad (13)$$

Where $M_s(t_i)$ and $\hat{M}_s(t_i, \theta)$ represent the measured and estimated magnetization, respectively. The optimal parameter vector is obtained solving $\hat{\theta}_{GA}^{n} = \min(ff(\theta))$ and also on a maximum allowed number of generations. Figure 1 shows the variation of the function of adaptation (fitness) according to the number generations, and table 1 give the final results of the genetic algorithm.

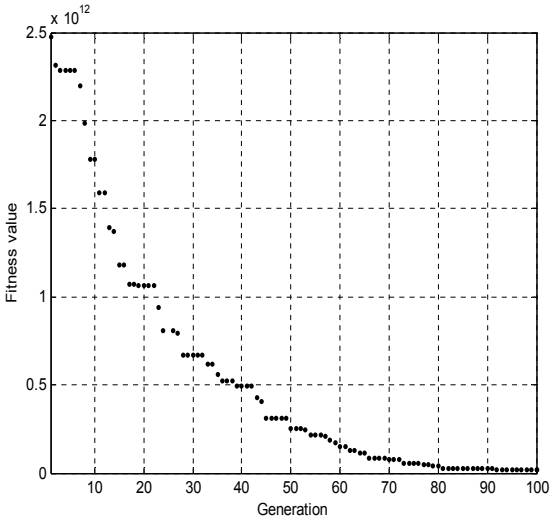

Figure 1. Evolution of the total error

TABLE 1
MATERIAL PARAMETERS

Parameter	Design Variable Range	Optimized Values
Ms	$0.5\times10^6 - 2.5\times10^6$	1.2865×10^6
k	75 - 450	195.68
c	0.15 – 0.65	495×10^{-3}
a	120 - 750	195.2
α	$1\times10^{-4} - 3\times10^{-4}$	1.75×10^{-4}

3.3 Artificial Neural Networks

3.3.1 Introduction

An artificial neural network is a directed graph (Figure 2) which is based on the organization of neurons in the human brain, in which many processors called cells or neurons, are able to perform basic calculations [13], [17]. These neurons are organized in layers that can exchange information via connections (synapses) between them.

3.3.2 Modeling of Hysteresis Loop by Multilayer Neural Networks

Our multi-layer neural network used is composed of three layers and driven by the *Levenberg-Marquard* algorithm, is implemented in *Matlab* to model the hysteretic behavior of a device formed of a ferromagnetic core inductor surrounding a non-linear. This algorithm is more efficient in terms of computation time than the simple gradient descent of the classical backpropagation.

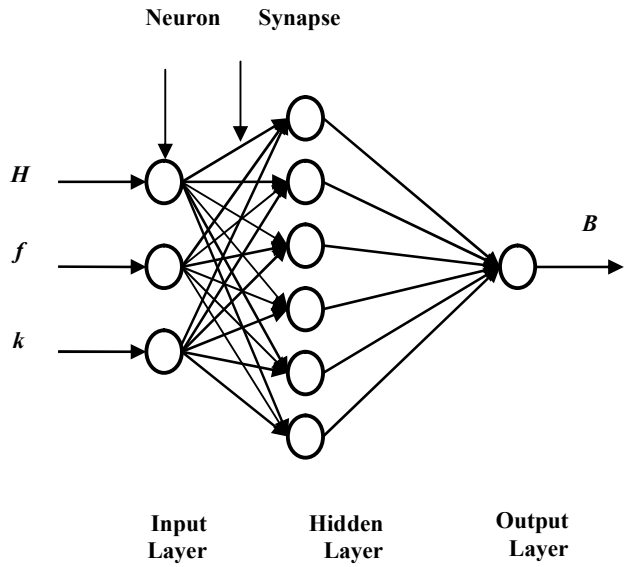

Figure 2. Structure of a proposed neural network

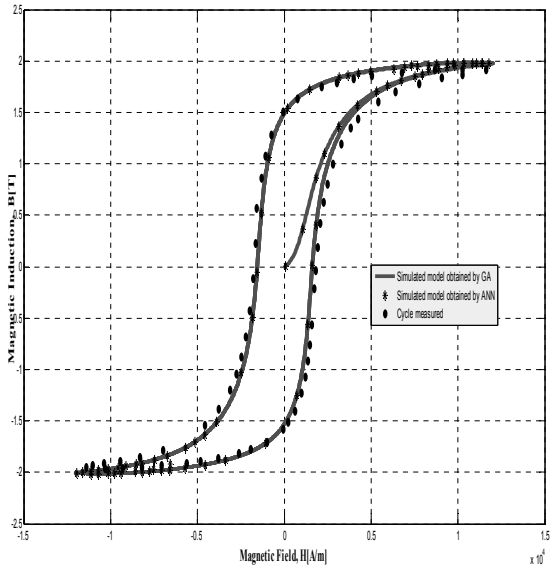

Figure 3. Validation of the hysteresis loop obtained by genetic algorithm and neural network

The first layer of the neural network consists of three units with a sigmoid activation function, the second layer consists of six units with a sigmoid activation function, and the third layer consists of a single unit with a function linear activation. The inputs of the network are the magnetic field ***H*** and the frequency or temperature, the third unit is a simple indicator of the evolution of the magnetic field, it takes the value 1 for an ascending field and the value 2 for a field down. However, the network returns the value of the magnetic induction ***B***.

The third unit in the input layer can particularize the hysteresis loop in each rectangle of the mesh taking into account the extreme values of the magnetic field. The maximum values of the magnetic field in each rectangle, necessary for learning of the neural network are calculated during the transient associated with the initial magnetization curve. The coefficient of relaxation ω ensuring the convergence is 10^{-4}. Numerical simulation (step by step in time) of the magnetic behavior is used to calculate the magnetic induction in each rectangle.

For validation of the parameters obtained, was superimposed on the figure 3 the experimental cycle obtained by § 4.1 and the cycle simulation obtained from the identified parameters. This overlay shows the accuracy of the cycle identified by genetic algorithm. We note that the difference between the measured and the simulated cycle is shown, which is reflected by value of the LSE error (Figure 3). It can also be noted that the cycle is symmetric.

This slight increase in the gap between simulation and experiment with refining the mesh can be explained by the existence of two sources of error inherent in the numerical model used for this study

- The modelling error which is the difference between the real system and mathematical model
- The numerical error which is the difference between the numerical model and the mathematical model.

The simulation results show that a neural network can accurately identify stable, non-linear relationship linking the variables together. The intrinsic characteristics of the latter have allowed us to have a very general model that can take into account all the factors that can affect the hysteresis cycle. Another advantage of this model is that it is designed from the experimental curves very near to reality.

3.4 The Solution Procedure

3.4.1 Introduction

Since their introduction in the sixties and early work on them, finite volume methods have continued to be a strong interest in several sub-disciplines of physics (thermodynamics, fluid mechanics ...). In fact, this method has been an important step not only for the modeling of fluid mechanics, but also for modeling other branches of engineering science: electromagnetic, heat transfer... etc [14]. The finite volume method is to integrate, on elementary volumes, the equations written in integral form. This method is particularly well adapted to the spatial discretization of conservation laws, in contrast to finite element, and is thus applicable in electromagnetism. Its implementation is simple if the elementary volumes or "control volumes" are rectangles in 2D or 3D parallelepipeds. However, the finite volume method allows the use of volumes of any shape and therefore to treat complex geometries, in contrast to finite differences. The computational domain is divided into a number of non-overlapping control volumes such that each volume around each point of the mesh (see figure 4).

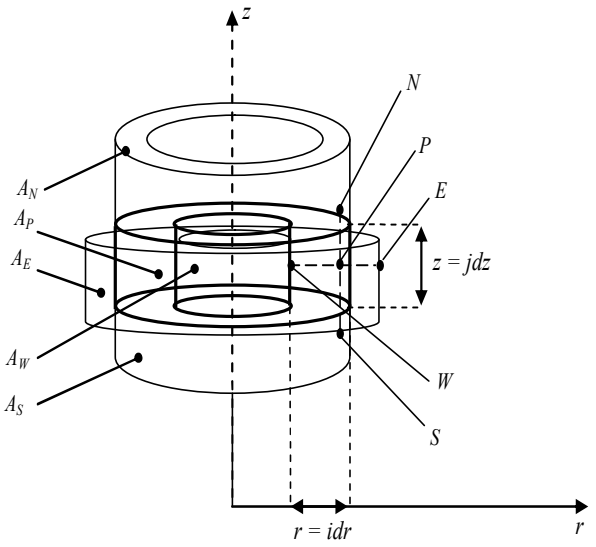

Figure 4. Control volume in axi-symmetrical cylindrical coordinates

3.4.2 Proposed Resolution Algorithm

The differential equation is integrated for each control volume of arbitrary expressions is chosen to express the variation of $\boldsymbol{A}$ between different points of the mesh and allow integration. The result of this integration gives the equation expressed using discrete values of the function $\boldsymbol{A}$ for a set of points of the mesh.

The discrete equation obtained expresses the conservation principle for $\boldsymbol{A}$ on the volume control in the same way that the differential equation expresses it for an infinitesimal control volume.

For this purpose let us multiply the equation magnetodynamic (equation 5) by the projection function βi and integrate the resulting equation on the domain Ω [15] [16], we obtain:

$$\int_t^{t+\Delta t}\iint_r\iint_z \beta_i\left[\frac{\partial}{\partial z}\left(\frac{1}{r\mu_0}\frac{\partial \boldsymbol{A}}{\partial z}\right)+\frac{\partial}{\partial r}\left(\frac{1}{r\mu_0}\frac{\partial \boldsymbol{A}}{\partial r}\right)\right] rdrdzdt =$$
$$\int_t^{t+\Delta t}\iint_r\iint_z \beta_i\left[\frac{\sigma}{r}\frac{\partial \boldsymbol{A}}{\partial t}-\boldsymbol{J_{ex}}\right] rdrdzdt \qquad (14)$$
$$+\int_t^{t+\Delta t}\iint_r\iint_z \beta_i\left(\frac{\partial \boldsymbol{M_r}}{\partial z}-\frac{\partial \boldsymbol{M_z}}{\partial r}\right) rdrdzdt$$

With B_i is function of selected projection *1/r*.

One can write (14) as

$$\int_t^{t+\Delta t}\iint_r\iint_z \left[\frac{\sigma}{r}\frac{\partial \boldsymbol{A}}{\partial t}-\frac{\partial}{\partial z}\left(\frac{1}{r\mu_0}\frac{\partial \boldsymbol{A}}{\partial z}\right)-\frac{\partial}{\partial r}\left(\frac{1}{r\mu_0}\frac{\partial \boldsymbol{A}}{\partial r}\right)\right] drdzdt =$$
$$\int_t^{t+\Delta t}\iint_r\iint_z \left[\boldsymbol{J_{ex}}+\frac{\partial \boldsymbol{M_z}}{\partial r}-\frac{\partial \boldsymbol{M_r}}{\partial z}\right] drdzdt \qquad (15)$$

After integration, the equation (15) discretized once is written as follows

$$\left(\begin{array}{l}\frac{\nu_0}{r_e}\frac{\Delta z\,\Delta t}{(\delta r)_e}+\frac{\nu_0}{r_w}\frac{\Delta z\,\Delta t}{(\delta r)_w}+\frac{\nu_0}{r_n}\frac{\Delta r\,\Delta t}{(\delta r)_n}+\\ \frac{\nu_0}{r_s}\frac{\Delta r\,\Delta t}{(\delta r)_s}+\frac{\sigma_P}{r_P}\Delta r\,\Delta z\end{array}\right) A_P$$
$$-\left(\begin{array}{l}\frac{\nu_0}{r_e}\frac{\Delta z\,\Delta t}{(\delta r)_e}A_E+\frac{\nu_0}{r_w}\frac{\Delta z\,\Delta t}{(\delta r)_w}A_W+\\ \frac{\nu_0}{r_n}\frac{\Delta r\,\Delta t}{(\delta r)_n}A_N+\frac{\nu_0}{r_s}\frac{\Delta r\,\Delta t}{(\delta r)_s}A_S\end{array}\right) \qquad (16)$$
$$+\frac{\sigma_P}{r_P}A_P(t+\Delta t)\Delta r\,\Delta z = J_S\,\Delta r\,\Delta z\,\Delta t$$
$$+\left[(M_z)_e-(M_z)_w\right]\Delta z\,\Delta t$$
$$-\left[(M_r)_n-(M_r)_s\right]\Delta r\,\Delta t$$

The equation (16) discretized once is written as follows

$$a_P A_P = a_E A_E + a_W A_W + a_N A_N + a_S A_S + d_0$$
$$+\frac{\sigma_p \Delta r\Delta z}{r_p\Delta t}A_p^0+\left[(M_z)_e-(M_z)_w\right]\Delta z \qquad (17)$$
$$-\left[(M_r)_n-(M_r)_s\right]\Delta r$$

The indices *P*, *W*, *N*, *E* and *S* refer to the values of the nodes and indices *p*, *w*, *n*, *e* and s refer to the values of the faces of volumes of control (See figure. 4).

The coefficients a_W, a_N, a_E, a_S and d_0 is given by

$$a_E=\frac{\Delta z}{\mu_0 r_e(\delta r)_e},\quad a_W=\frac{\Delta z}{\mu_0 r_w(\delta r)_w},$$
$$a_N=\frac{\Delta r}{\mu_0 r_n(\delta z)_n},\quad a_S=\frac{\Delta r}{\mu_0 r_s(\delta z)_s}, \qquad (18)$$
$$a_P=a_E+a_W+a_N+a_S+\frac{\sigma_P}{r_P}\frac{\Delta r\Delta z}{\Delta t},$$
$$d_0=J_{ex}(t)\Delta r\Delta z.$$

$$a_P=a_E+a_W+a_N+a_S+\frac{\sigma_P}{r_P}\frac{\Delta r\Delta z}{\Delta t},$$
$$d_0=J_{ex}(t)\Delta r\Delta z.$$

Once the various formulations including finite volume model of hysteresis are established, a method for solving the nonlinear problem must be chosen. In the literature, several algorithms are proposed to solve the nonlinear problem such as the *Newton-Raphson* method or the direct method called fixed point method (FPM).

Finally, the partial differential equation (5) becomes

$$curl\,\nu_{FP}\;curl\,A = J - curl\,M_{FP} \qquad (19)$$

The discretization with nodal shape functions for the potential vector of (19) using the finite volume method leads to the matrix system

$$[S_{FP}][A]=[J]-[M_{FP}] \qquad (20)$$

Where the vector [*A*] represents the nodal values of vector potential. [***SFP***] a square matrix called stiffness matrix, [***MFP***] and [***J***] the vectors which take into account the magnetization *MFP* and the current density ***J***. a vector [*D*] is introduced such that [***J***] = [*D*] ***i***. Then, we obtain the matrix system [17]:

$$\begin{bmatrix}\boldsymbol{S_{FP}} & -D\\ 0 & R\end{bmatrix}\begin{bmatrix}\boldsymbol{A}\\ \boldsymbol{i}\end{bmatrix}+\begin{bmatrix}0 & 0\\ D^t & 0\end{bmatrix}\frac{d}{dt}\begin{bmatrix}\boldsymbol{A}\\ \boldsymbol{i}\end{bmatrix}$$
$$=\begin{bmatrix}0\\ u\end{bmatrix}+\begin{bmatrix}\boldsymbol{M_{PF}}\\ \boldsymbol{0}\end{bmatrix}. \qquad (21)$$

In this work, we used the so-called fixed point method described by the direct algorithm of Table 2 in below. This is motivated by the major advantage offered by this algorithm, avoiding the calculation of derivatives.
The fixed point method using the model of hysteresis in its forward or reverse is distinguished by its ease of implementation. As the reversal of the model has an additional cost in terms of computation time, we opted for the use of fixed-point method with the direct model of hysteresis associated with a new algorithm for solving the problems of convergence. This algorithm will be presented with the study of the choice of relaxation factor and verification of convergence at critical points of the hysteresis loop [16] [17].

TABLE 2: Iterative Steps Algorithm

1. Initialization : t=1 (time), i=1(space), give ε
2. Numerical code from control volume
2.1. Initialization : $\overrightarrow{M^i}$
2.2. $\sigma\frac{\partial\overrightarrow{A^i}}{\partial t}+\vec{\nabla}\times\left(\frac{1}{\mu_0}\vec{\nabla}\times\overrightarrow{A^i}\right)=\vec{J}_S-\vec{\nabla}\times\overrightarrow{M^i}\left(\overrightarrow{A^i}\right)$
2.3. $\left\|\overrightarrow{B^i}\right\|=\left\|\vec{\nabla}\times\overrightarrow{A^i}\right\|$
2.4. $H_s^i=\frac{B_s^i}{\mu_0}-M^i$
2.5. $H_s^i=\omega.H_s^i+(1-\omega).H_s^{i-1}$ relaxation coefficient
2.6. $M_s^i=f\left(H_s^i\right)$ from *Jiles-Atherton* hysteresis model
2.7. Calculate the direction of M_s^i
2.8. Calculate the precision τ
2.9. If $\tau\le\varepsilon\Rightarrow$ convergence : $t=t+1$ et $i=i+1$ go to 2.1, else $i=i+1$ go to 2.2
3. Results

4. RESULTS

4.1 Measured Curves

The determination of the magnetic quality of materials rests primarily on the nature of the systems of measurement used. The evolution of the standard in the field of the characterization of material is a significant factor for the taking into account of the physical nature of magnetic materials and the conditions of their uses. The reproducibility of measurement and the facility of handling are also factors which make it possible to choose the type of magnetic circuit to implement. Accordingly our choice is related to the realization of framework SST (Single Sheet Tester) 500 mm*500 mm (See figure 5) [18], [19].
The device planned for characterization of sheets with not oriented grains must make it possible to take measurements by a simple introduction of the sample, iron silicon 3% not oriented inside a sleeve, with a perfect positioning and without deterioration of the polar faces of the magnetic circuit of closing of flux. The characterization of materials studied done by determining the following quantities expressed in terms of characterization of the frame and measuring output voltages measured by an oscilloscope: V_2, V_{H1}, and V_{H2}.
The excitation peak field, which is submitted the sample is obtained by interpolation from tensions measured at the terminals of two coils tangential H_1 and H_2 located at distances different from the sample

$$\frac{dH(t)}{dt}=\frac{d_2}{d_2-d_1}\frac{dH_1(t)}{dt}-\frac{d_1}{d_1-d_2}\frac{dH_2(t)}{dt} \quad (22)$$

Where

$$\frac{dH_1(t)}{dt}=\frac{V_{H1}(t)}{\mu_0 n_1 S_1} \quad (23)$$

And

$$\frac{dH_2(t)}{dt}=\frac{V_{H2}(t)}{\mu_0 n_2 S_2} \quad (24)$$

The magnetic induction is obtained by time integration of the V_2 *(t)* voltage in secondary coil measuring ***B*** by

$$B_{\exp}(t)=\frac{\overline{V_2}}{4 N_2 S f} \quad \text{And} \quad \overline{V_2}=\frac{1}{T}\int_0^T V_2(t)\,dt \quad (25)$$

Where

d_1, d_2: Distance to sample the coil Field 1, 2 (m).
N_2: Number of turns of the coil measuring ***B***.
n_1, n_2: Number of turns of the coil Field *N° 1, N° 2.*
S: Section of the sample (m^2).
S_1, S_2: Surface of the coil H_1, H_2 (m^2).
V_{H1}, V_{H2}: power output of the coil H_1, H_2 (V).

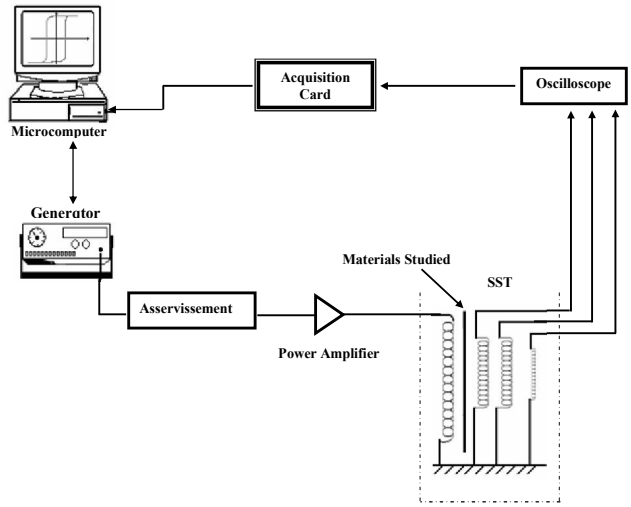

Figure 5. Single sheet Tester (SST), 500mm*500 mm

It is important to note that the use of inverse model of *J-A* for the identification of parameters in an additional advantage over the original model: the input of the inverse model is the form of magnetic induction wave. Since the magnetic induction is obtained from the integration, it is naturally filtered with fewer oscillations than the waveform of the magnetic field. The noise in the waveform on the ground brings additional difficulties for parameters identification procedure. All parameters obtained are valid for models, original and reverse, allowing a good agreement between measured and calculated data.

4.2 Comparison with Simulation

4.4.1 Introduction

We propose in this section a validation of the computer code and the integration algorithm of the hysteresis model. In the work carried out within our laboratory, a device has been proposed in order to compare results from different platforms simulation. This device consists of a sheet of FeSi 3% characterized in the following paragraph. The dimensions of this device are given in figure 6.

4.4.2 Validation of Results

The test consists of a cylinder ferromagnetic with a length of ***40 cm*** and ***10 cm*** diameter characterized by a cycle of hysteresis *(Ms*=1.2865×10^6*, k*=195.68*, c*=495×10^{-3}*, a=1*95.2*, α*=1.75×10^{-4}*)*, the cylinder is surrounded by a coil of the same length traversed by a stream of density $J =$ ***10^5 A/m^2***. The drivers which constitute the inductor have a diameter D ***= 1 cm*** and ***50 cm*** length. The gap is E ***= 2 cm***. The geometry of the system studied, it presents two symmetries, the first axially (*oz*) and the second according to the plan (*or*). We can then consider magnetic problem in a cylindrical coordinate system, a quarter of domain. For a numerical modelling the theoretical limits (with infinite, ***A = 0***) are brought back to a finite distance which can vary according to the desired precision. In this study, these limits were fixed at a distance L ***= 50 cm*** of the studied device.

The boundary conditions associated with the magnetic equation are the conditions of *Neumann* $\partial A/\partial n = 0$ and the conditions of the *Dirichlet* ***A****=0* of representing in figure 6.

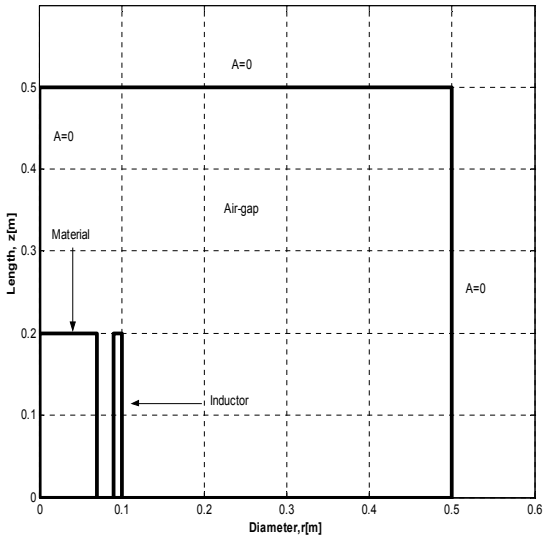

Figure 6. Field of study of the axi-symmetrical problem with boundary conditions

We have defined in this geometry three reference points on which we will determine the waveform of the field, the magnetic induction, the hysteresis loop and the magnetic vector potential driven. Based on the system axis (r, z) defined in figure 6, the coordinates of these points are defined as P1 (6, 10) cm, P2 (5, 5) cm, and P3 (3, 7) cm.

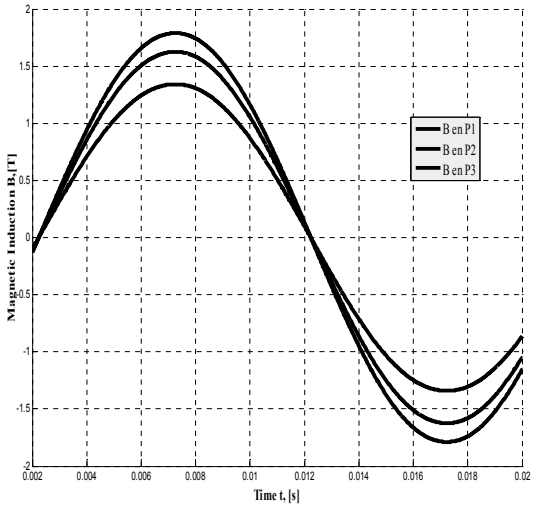

Figure 7. Flux density variations

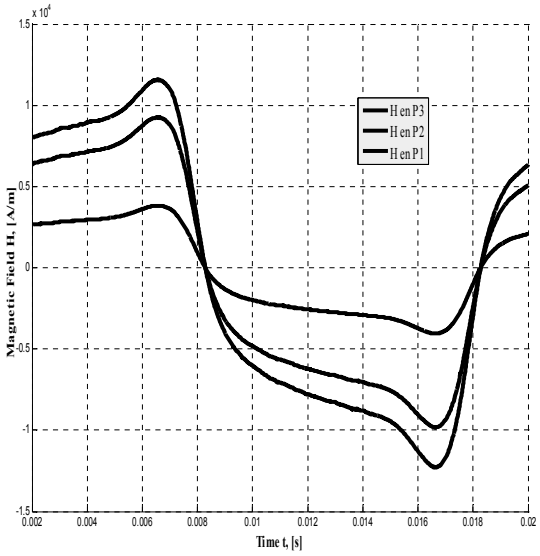

Figure 8. Simulated field versus time curve

Numerical simulation (step by step in time) of the magnetic behavior of the device study reveals that the magnetic flux density is nearly sinusoidal at all points of figure 7 of ferromagnetic sample. Unlike the magnetic induction, the magnetic field is greatly distorted. In figure 8 we can distinguish this distortion and the delay introduced by the hysteresis between the field and the magnetic induction. The hysteresis loops described previously defined points are shown in figure 9.

The hysteresis loops (each mesh element), described in previously defined points exhibit better consistency and thus the good modeling of the measured hysteresis neural-genetic approach. The saturation magnetization should be different because of the location of benchmarks by the heart of the inductor report.

Comparing these results with other previous work [20] [21], we find that we made a big improvement on the accuracy of the

identified parameters, and therefore we can say that these results are good and acceptable.

For an operation frequency of 50 Hz, the experimental and simulated field curves of this material FeSi 3% when submitted to a 1.98 T peak value sinusoidal induction (See figure 3).

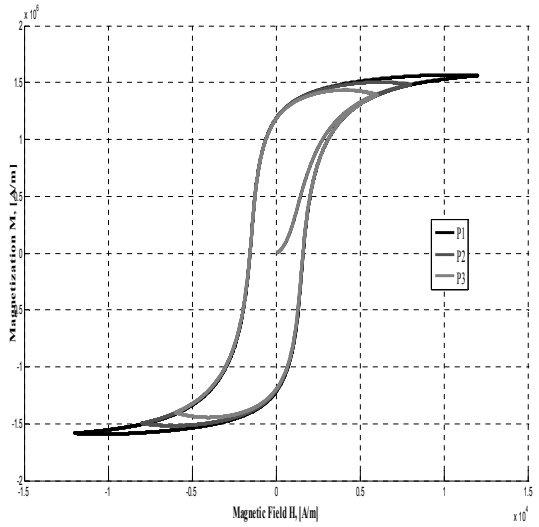

Figure 9. Hysteresis loops calculated

Additional resultants are given in figure 10, where the axial variations of potential vector magnetic ***A***. One notices well that the value of ***A*** is maximal on the level of the center of the inductor then decreases gradually until being cancelled in extreme cases of the field of study.

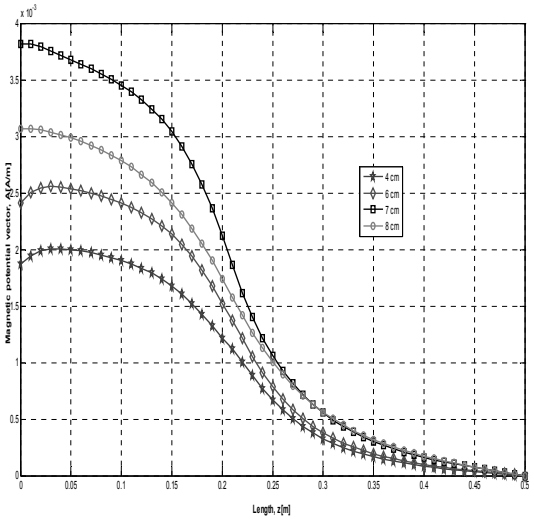

Figure 10. Axial variation of the magnetic potential vector *A*

5. CONCLUSION

Through this work, we tried to implement the means to incorporate the hysteresis phenomenon in a two-dimensional modeling of the magnetic field in static electrical devices. The *Jiles-Atherton* model is a physical model of magnetic hysteresis. It is valid for the characterization of soft ferromagnetic materials such as steels used in electrical construction. The hysteresis loop of the *Jiles-Atherton* model is very sensitive to the variation of its parameters. The identification of parameters of *Jiles-Atherton* model is a difficult process to achieve, but the use of optimization techniques (genetic algorithm) is used to free this difficulty.

In this paper, we tried to introduce new techniques in the calculation for economy of electromagnetic computation time and the development of realistic models and the exact determination of the parameters appear as major criteria. So, we proposed a neural model for modeling the hysteresis loop, this model has allowed us to introduce the different behaviors of the influential external hysteresis loop (frequency, temperature…). The results of these variations given by our neural model are more near to realty that the learning cycle was performed on the basis of reported experimental. As such, this model has been integrated in finite volume coded.

The objective of our work is the application of alternative methods (neuro-genetic) to relieve the heavy digital calculated based on the standard mesh each time the hysteresis model.

All results obtained by applying our model to axisymmetric magneto device based on a *Jiles-Atherton* inverse model and differential reluctivité to good performance for digital convergence and give very satisfactory results with SST data frame.

In near work, using a dynamic model of the magnetic hysteresis to study the material behavior in systems with high frequency, integrate the model into a finite element computer coded coupling the resolution of *Maxwell*'s equations to those equations of heat and power (inclusion of a power supply) and application to other devices will be provided.

REFERENCES

[1] H. L. Toms, R. G. Colclaser, M. P. Krefta, "Tow Dimensional Finite Element Magnetic Modeling for Scalar Hysteresis Effects," IEEE Transaction on Magnetics, vol. 37, pp 982-988, March. 2001.

[2] N. Sadowski, N. J. Batistela, J. P. A. Bastos, and M. Lajoie-Mazenc, "An Inverse Jiles–Atherton Model to Take Into Account Hysteresis in Time-Stepping Finite-Element Calculations," IEEE Transaction on Magnetics., vol. 38, pp 797-800, March. 2002.

[3] D. C. Jiles and D. L. Atherton, "Theory of ferromagnetic hysteresis," Journal of Magnetism and Magnetic Materials, vol. 61, pp. 48–60, 1986.

[4] Krzysztof Chwastek, "Description of Henkel Plots by the Magnetization-Dependent Jiles-Atherton Model," Journal of Magnetism and Magnetic Materials, vol. 322, Issue 2, pp. 214-217, January.2010.

[5] Wei Li , In Hyun Kim , Seok Myeong Jang, and Chang Seop Ko "Hysteresis Modeling for Electrical Steel Sheets Using Improved Vector Jiles-Atherton Hysteresis Model," IEEE Transaction on Magnetics, vol. 47, pp 3821-3824, October.2011.

[6] Krzysztof Chwastek, Jan Szczygłowski, "An Alternative Method to Estimate the Parameters of Jiles-Atherton Model," Journal of Magnetism and Magnetic Materials, vol. 314, Issue 1, pp. 47-51, July 2007.

[7] J. V. Leite, S. L.Avila, and others, "Real Coded Genetic Algorithm for Jiles-Atherton Model Parameters Identification," IEEE Transaction on Magnetics, vol. 34, pp 888-891, March.2004.

[8] J. A. Vasconcelos, J. A. Ramirez, R. H. C. Takahashi, R. R. Saldanha, “Improvements in Genetic Algorithms,” IEEE Transaction on Magnetics, vol. 37, pp 3414-3417, September. 2001.

[9] P. R. Wilson, N. Ross, A. D. Brown, “Optimizing the Jiles-Atherton Model of hysteresis by a Genetic Algorithm,” IEEE Transaction on Magnetics, vol. 37, pp 989-993, March. 2001.

[10] B. Gallardo, D. A. Lowther, “Some Aspects of Niching Genetic Algorithms Applied to Electromagnetic Device Optimization,” IEEE Transaction on Magnetics, vol. 36, pp1076-1079, July. 2000.

[11] K. Chwastek, J. Szczyglowski, “Identification of a Hysteresis Model Parameters with genetic Algorithms,” Journal of Mathematics and Computers in Simulation, vol. 71, pp. 206-211, 2006.

[12] L. A. L. Almeida, G.S. Deep, A.M.N. Lima and H. Neff, “Modeling a magnetostrictive transducer using genetic algorithm,” Journal of Magnetism and Magnetic Materials, vol. 266-230, pp. 1262-1264, 2001.

[13] M. Kuczmanne and A.Iványi, “A New Neural-Network-Based Scalar Hysteresis Model,” IEEE Transaction on Magnetics, vol. 38, pp 857-860, March. 2002.

[14] S. V. Patankar, “Numerical Heat Transfer and Fluid Flow,” Series in computational methods in mechanics and thermal sciences.

[15] S. Azzaoui, K. Srairi, “Nonlinear Magnetic Modeling by FVM for Jiles-Atherton Hysteresis Model Using a Genetic Algorithm Parameter’s Identification”, JEE Journal of Electrical Engineering, vol. 9, No. 3, pp. 9-15, Sep 2009.

[16] S. Azzaoui, K. Srairi, M.E.H. Benbouzid, “Finite Volume Magnetic Modeling for Jiles-Atherton Scalar Hysteresis Model Optimizing by a Genetic Algorithm”, JES Journal, Journal of Electrical Systems, vol. 5, Issue 2, pp. 01-13, Juin 2009.

[17] Seddik Azzaoui, Kamel Srairi, Mohamed El Hachemi Benbouzid, " Non Linear Magnetic Hysteresis Modelling by Finite Volume Method for Jiles-Atherton Model Optimizing by a Genetic Algorithm ". JEMAA, Journal of Electromagnetic Analysis and Applications, vol. 3, Issue 6, pp. 191-198, Juin 2011.

[18] Tom Hilgert, Lieven Vandevelde, and Jan Melkebeek, Tom Hilgert, Lieven Vandevelde, and Jan Melkebeek, “Neural-Network-Based Model for Dynamic Hysteresis in the Magnetostriction of Electrical Steel Under Sinusoidal Induction,” Transaction on Magnetics, vol. 43, pp3462-3466, August 2007.

[19] Tsakani Lotten Mthombeni, “Improved Lamination Core Loss Measurements and Calculations”, (Thesis of Doctorate), Clarkson University, April 10, 2006.

[20] Paolo Del Vecchio, and Alessandro Salvini, “Neural Network and Fourier Descriptor Macromodiling Dynamic Hysterisis”, IEEE Transaction on Magnetics, vol. 36, No. 36, pp. 1246-1249, July. 2000.

[21] Tom Hilgert, Lieven Vandevelde, and Jan Melkebeek; “Neural-Network-Based Model for Dynamic Hysteresis in the Magnetostriction of Electrical Steel under Sinusoidal Induction”, IEEE Transaction on Magnetics, vol. 43, No.8, pp. 1076-1079, August. 2007.